Superconducting quantum bits

John Clarke[1,2] & Frank K. Wilhelm[3]

Superconducting circuits are macroscopic in size but have generic quantum properties such as quantized energy levels, superposition of states, and entanglement, all of which are more commonly associated with atoms. Superconducting quantum bits (qubits) form the key component of these circuits. Their quantum state is manipulated by using electromagnetic pulses to control the magnetic flux, the electric charge or the phase difference across a Josephson junction (a device with nonlinear inductance and no energy dissipation). As such, superconducting qubits are not only of considerable fundamental interest but also might ultimately form the primitive building blocks of quantum computers.

The theory of quantum mechanics was originally developed to account for the observed behaviour of electrons in atoms. More than 80 years later, it is being used to explain the behaviour of superconducting circuits that can be hundreds of nanometres wide and can contain trillions of electrons. The quantum nature of these circuits is observable because they can be engineered to be isolated from the electrical environment and are thus represented by a single degree of freedom. Significant coupling to other degrees of freedom causes rapid decoherence, destroying the quantum state of the circuit so that it behaves classically. Unlike atoms, these circuits can be designed and constructed to tailor their characteristic frequencies, as well as other parameters. These frequencies can be controlled by adjusting an external parameter, and the coupling energy between two quantum bits (qubits) can be turned on and off at will.

Superconducting quantum circuits are the subject of intense research at present, in part because they have opened up a new area of fundamental science and in part because of their long-term potential for quantum computing. In this review, we begin with a brief discussion of superconductivity and two of the superconducting properties that underlie how qubits operate: flux quantization and Josephson tunnelling. The three fundamental types of superconducting qubit — flux, charge and phase — are then described. This is followed by a review of the real-time, quantum-coherent dynamics of qubits and the limitations imposed by relaxation and decoherence, as well as the mechanisms of decoherence. We then discuss schemes for controlling the coupling between two qubits, a feature that greatly simplifies the implementation of proposed quantum-computing architectures. And we finish by discussing quantum optics on a chip, a new research direction in which the electromagnetic fields associated with control and read-out signals are treated quantum mechanically.

Flux quantization and Josephson tunnelling

Why do superconductors enable atomic-scale phenomena to be observed at the macroscopic level? The reason, as explained elegantly by the theory of Bardeen, Cooper and Schrieffer[1], is that in a given superconductor all of the Cooper pairs of electrons (which have charge $2e$, mass $2m_e$ and spin zero, and are responsible for carrying a supercurrent) are condensed into a single macroscopic state described by a wavefunction $\Psi(\mathbf{r}, t)$ (where $\mathbf{r}$ is the spatial variable and t is time.) Like all quantum-mechanical wavefunctions, $\Psi(\mathbf{r}, t)$ can be written as $|\Psi(\mathbf{r}, t)| \exp[i\phi(\mathbf{r}, t)]$ (where $i = \sqrt{-1}$): that is, as the product of an amplitude and a factor involving the phase ϕ. Furthermore, in 'conventional'

superconductors such as Nb, Pb and Al, the quasiparticles (electron-like and hole-like excitations) are separated in energy from the condensate[2] by an energy gap $\Delta_s(T) = 1.76k_B T_c$ (where k_B is the Boltzmann constant and T_c is the superconducting transition temperature). Thus, at temperatures $T \ll T_c$, the density of quasiparticles becomes exponentially small, as does the intrinsic dissipation for frequencies of less than $2\Delta_s(0)/h$ (where h is Planck's constant) — roughly 10^{11} Hz for Al.

The macroscopic wavefunction leads to two phenomena that are essential for qubits. The first phenomenon is flux quantization. When a closed ring is cooled through its superconducting transition temperature in a magnetic field and the field is then switched off, the magnetic flux Φ in the ring — maintained by a circulating supercurrent — is quantized[2] in integer values of the flux quantum $\Phi_0 \equiv h/2e \approx 2.07 \times 10^{-15}$ T m^2. This quantization arises from the requirement that $\Psi(\mathbf{r}, t)$ be single valued. The second phenomenon is Josephson tunnelling[2]. A Josephson junction consists of two superconductors separated by an insulating barrier of appropriate thickness, typically 2–3 nm, through which Cooper pairs can tunnel coherently. Brian Josephson showed that the supercurrent I through the barrier is related to the gauge-invariant phase difference $\delta(t)$ between the phases of the two superconductors by the current–phase relationship

$$I = I_0 \sin\delta \qquad (1)$$

Here I_0 is the maximum supercurrent that the junction can sustain (that is, the critical current). This phase difference is an electrodynamic variable that, in the presence of a potential difference V between the superconductors, evolves in time as

$$\hbar\dot{\delta} = \hbar\omega = 2eV \qquad (2)$$

where $\hbar = h/2\pi$ and ω is the angular frequency at which the supercurrent oscillates. The dynamical behaviour of Josephson junctions is described in Box 1.

The variables have, so far, been regarded as being classical, but to show quantum-mechanical behaviour, these variables must be replaced by operators. The two relevant operators are that for δ, which is associated with the Josephson coupling energy $E_J \equiv I_0\Phi_0/2\pi$, and that for the Cooper-pair number difference N across the capacitance, which is associated with the charging energy $E_c \equiv (2e)^2/2C$, where C is the junction capacitance.

Furthermore — just like the familiar position and momentum operators x and p_x — the operators for δ and for the charge on the capacitor Q

Box 1 | The Josephson junction as a nonlinear circuit element

a

b
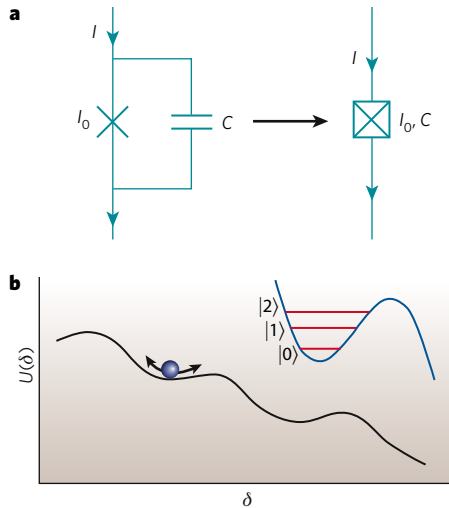
Equations (1) and (2) contain the crucial information that the Josephson junction is a dissipationless device with a nonlinear inductance. It is these unique features that make the junction the primitive building block of all superconducting qubits.

The nonlinear inductance is easily deduced by noting that the time derivative of equation (1) yields $\dot{I} = (I_0\cos\delta)\dot{\delta} = (I_0\cos\delta)\omega = V(2eI_0/\hbar)\cos\delta$ from equation (2). Invoking Faraday's law $V = -L\dot{I}$ (where L is the inductance) then leads to the Josephson inductance

$$|L_j| = \Phi_0/(2\pi I_0\cos\delta) = \Phi_0/2\pi(I_0^2 - I^2)^{1/2} \text{ (where } I < I_0) \tag{6}$$

The Josephson junction, denoted by an X in panel **a** of the figure, has an intrinsic capacitance C; this combination is often denoted by an X in a box. I_0 denotes the critical current. It is immediately apparent from equation (6) that the junction is also a nonlinear oscillator with a resonant angular frequency $\omega_p(I) = (L_jC)^{-1/2} = (2\pi I_0/\Phi_0 C)^{1/2}/(1 - I^2/I_0^2)^{1/4}$.

Considerable insight into the dynamics of a Josephson junction can be gleaned by considering the flow of a current J through the junction: $J = I_0\sin\delta + C\dot{V}$. Writing $\dot{V} = (\hbar/2e)\ddot{\delta}$ and rearranging this yields $(\hbar C/2e)\ddot{\delta} = I - I_0\sin\delta = -(2e/\hbar)\partial U/\partial\delta$. $U \equiv -(\Phi_0/2\pi)\partial U/\partial\delta$ is the potential of a tilted washboard for a particle of mass $\hbar C/2e$ (as illustrated in panel **b** of the figure). In the absence of fluctuations, for $I < I_0$ the particle remains trapped in one of the potential wells; classically, it oscillates in the well at the plasma oscillation frequency $\omega_p(I)/2\pi$. Thus, $\langle\delta\rangle = 0$, and the junction is in the zero-voltage state; in the quantum picture, the energy in the well is quantized, as shown in the inset (figure, panel **b**). By contrast, when I is increased so that $I > I_0$, the particle runs down the washboard, $\langle\dot{\delta}\rangle > 0$, and there is a voltage across the junction. When I is subsequently reduced so that $I < I_0$, the particle will continue to propagate until I is close to 0. Thus, the current–voltage characteristic is hysteretic.

are canonically conjugate, as expressed by the commutator bracket $[\delta, Q] = i2e$. The fact that δ and Q are subject to Heisenberg's uncertainty principle has far-reaching consequences. On the one hand, when $E_j >> E_c$, δ is well defined, and Q has large quantum fluctuations; therefore, the Josephson behaviour of the junction dominates. On the other hand, when $E_j << E_c$, N is well defined, and δ has large quantum fluctuations; therefore, the charging behaviour of the capacitor dominates. Using these ideas, the parameters of superconducting quantum circuits can be designed[3].

The first evidence of quantum behaviour in a Josephson junction came from experiments in which macroscopic quantum tunnelling was found to occur and energy levels were shown to be quantized. In macroscopic quantum tunnelling[4,5], the junction tunnels from the ground state $|0\rangle$ (Box 1 figure), when $I < I_0$, through the potential barrier that separates it from its neighbouring energy well, which is at a lower energy. Then, the particle runs freely down the washboard potential,

generating a voltage $2\Delta_s/e$ that is readily detected. These results[5] were found to be in strong agreement with theory[6]. Energy quantization[7] was found in the initial well by irradiating the junction with microwaves. The escape rate from the zero-voltage state was increased when the microwave frequency f_m corresponded to the energy difference between two adjacent energy levels. A crucial point is that the anharmonic nature of the well, which results from the nonlinear inductance of Josephson junctions (equation (6), Box 1), causes the energy spacing to decrease as the quantum number progressively increases, so each transition has a distinct frequency. If the well were harmonic, the energy spacings would be identical, and the quantum case would not be distinguishable from the classical case.

These experiments showed unequivocally that δ is a quantum variable. The next step in the demonstration of macroscopic quantum physics was to implement devices showing the superposition of two quantum states $|\Psi_1\rangle$ and $|\Psi_2\rangle$ in the form $|\Psi\rangle = \alpha|\Psi_1\rangle + \beta|\Psi_2\rangle$, as first proposed by Anthony Leggett[8] in the 1980s in his discussion of macroscopic quantum coherence in superconducting devices. In 1997, Yasunobu Nakamura et al.[9] carried out the first such experiment on a charge qubit, showing spectroscopically the superposition of the Cooper-pair states $|n\rangle$ and $|n+1\rangle$, where the integer n is the quantum number specifying the number of Cooper pairs. Subsequently, in 2000, Jonathan Friedman et al.[10] and Caspar van der Wal et al.[11] showed the superposition of states in a flux qubit. A flux qubit consists of a superconducting loop interrupted by one[10] or three[11] Josephson junctions. The two quantum states are flux pointing up and flux pointing down or, equivalently, supercurrent flowing in an anticlockwise direction and supercurrent flowing in a clockwise direction. In 2002, Denis Vion et al.[12] described 'quantronium', a qubit in which two small junctions are connected by a superconducting island, involving the superposition of the Cooper-pair states $|n\rangle$ and $|n+1\rangle$. Also in 2002, John Martinis et al.[13] demonstrated a phase qubit, a reinvention of the device used earlier to observe quantized energy levels[7]. The relevant quantum states are the ground state and the first excited state. Some of the experimental difficulties encountered when operating superconducting qubits are described in Box 2.

Flux qubits

A flux qubit, as indicated earlier, consists of a superconducting loop interrupted by one[10] or three[11] Josephson junctions (Fig. 1a). Although both designs function similarly, we focus on the three-junction design, which has been adopted more widely. In this device, one junction is smaller in area and thus has a smaller critical current than the other two, which function to increase the inductance of the loop. The small junction has a large value for E_j/E_c, typically 50, so the phase difference δ (or, equivalently, the magnetic flux Φ in the loop) is the relevant quantum variable. The two quantum states are magnetic flux pointing up $|\uparrow\rangle$ and magnetic flux pointing down $|\downarrow\rangle$ or, equivalently, anticlockwise qubit supercurrent I_q circulating in the loop and clockwise supercurrent. The qubit is represented by a double-well potential, which is generally asymmetrical. The two states are coupled by the quantum-mechanical tunnelling of δ through the barrier separating the wells, giving rise to the superposition of the two basis states

$$|\Psi\rangle = \alpha|\uparrow\rangle \pm \beta|\downarrow\rangle \tag{3}$$

When the externally applied magnetic flux $\Phi_e = \Phi_0/2$, the double-well potential becomes symmetrical (Fig. 1b), and the two eigenfunctions become symmetrical and antisymmetrical superpositions of the two basis states, with $\alpha = \beta = 1/\sqrt{2}$. At this degeneracy point, the splitting of the energy levels of the ground state $|0\rangle$ and the first excited state $|1\rangle$ is Δ; away from the degeneracy point, the energy difference is

$$\nu = (\Delta^2 + \varepsilon^2)^{1/2} \tag{4}$$

where $\varepsilon = 2I_q(\Phi_e - \Phi_0/2)$ (Fig. 1c). The probabilities of observing the states $|\uparrow\rangle$ and $|\downarrow\rangle$ in the ground and first excited states as a function

of Φ_e are shown in Fig. 1d. At the degeneracy point, the probability of observing either state is ½. As Φ_e is reduced, the probability of observing $|\uparrow\rangle$ increases while that of observing $|\downarrow\rangle$ decreases.

 The first observation of quantum superposition in a flux qubit was made spectroscopically. The state of the flux qubit is measured with a d.c. superconducting quantum interference device (SQUID)[14]. This device consists of two Josephson junctions, each with critical current I_0, connected in parallel on a superconducting loop of inductance L. The critical current of the SQUID $I_c(\Phi_s)$ is periodic in the externally applied magnetic flux Φ_s with period Φ_0. In the limit $\beta_L \equiv 2LI_0/\Phi_0 << 1$ in which the Josephson inductance dominates the geometrical inductance, the critical current for $\Phi_s = (m + ½)\Phi_0$ (m is an integer) is reduced to almost zero, and the flux dependence of the critical current takes the approximate form[14] $I_c(\Phi_s) \approx 2I_0|\cos(\pi\Phi_s/\Phi_0)|$. Thus, by biasing the SQUID with a constant magnetic flux near $\Phi_0/2$, and measuring the critical current, the changes in flux produced by a nearby qubit can be measured with high sensitivity. In most experiments with qubits, a pulse of current is applied to the SQUID, which either remains in the zero-voltage state or makes a transition to the voltage state, producing a voltage $2\Delta_s/e$. Because its current–voltage characteristic is hysteretic, the SQUID remains at this voltage until the current bias has been removed, allowing researchers to determine whether the SQUID has switched. For sufficiently small current pulses, the probability of the SQUID switching is zero, whereas the probability is one for sufficiently large pulses. The switching event is a stochastic process and needs to be repeated many times for the flux in the SQUID to be measured accurately.

 The first step in spectroscopic observation of quantum superposition is to determine the height of the current pulse at which the SQUID switches — with, for example, a probability of ½ — as a function of Φ_e over a narrow range (perhaps $\pm 5m\Phi_0$). Subsequently, a pulse of microwave flux is applied at frequency f_m, which is of sufficient amplitude and duration to equalize the populations of the ground state and first excited state when the energy-level splitting difference $v = hf_m$. Assuming that $|\uparrow\rangle$ is measured, then, on resonance, there will be a peak in the switching probability for $\Phi_e < \Phi_0/2$ and a corresponding dip for $\Phi_e > \Phi_0/2$. An example of these results[11,15] is shown in Fig. 2. The configuration of the qubit and the SQUID is shown in Fig. 2a, and the peaks and dips in the amplitude of the switching current
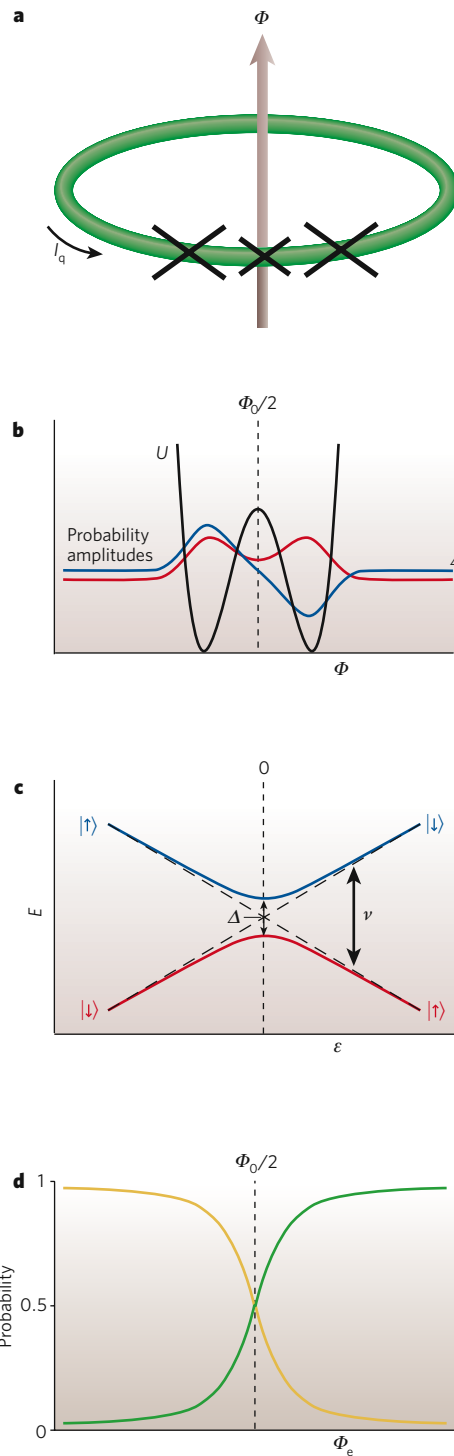
Figure 1 | The theory underlying flux qubits. a, Flux qubits consist of a superconducting loop interrupted by either one or three (shown) Josephson junctions. The two quantum states are magnetic flux Φ pointing up $|\uparrow\rangle$ and Φ pointing down $|\downarrow\rangle$ or, equivalently, supercurrent I_q circulating in the loop anticlockwise and I_q circulating clockwise. **b**, The double-well potential (black) versus total flux Φ contained in a flux qubit is shown. The two wells are symmetrical when the externally applied magnetic flux Φ_e is $(n + ½)\Phi_0$, where n is an integer (n = 0 in this case). The coloured curves are the eigenfunctions (probability amplitudes) for the ground state (symmetrical; red) and first excited state (antisymmetrical; blue). **c**, The energy E of the two superpositions states in **b** versus the energy bias $\varepsilon = 2I_q(\Phi_e - \Phi_0/2)$ is shown. The diagonal dashed black lines show the classical energies. The energy-level splitting is Δ at the degeneracy point, $\varepsilon = 0$, and is v for $\varepsilon \ne 0$. **d**, The probabilities of the qubit flux pointing up (green) or down (yellow) in the ground state versus applied flux are shown.

1033

Figure 2 | Experimental properties of flux qubits. a, The configuration of the original three-junction flux qubit is shown. Arrows indicate the current flow in the two qubit states (green denotes $|\uparrow\rangle$, and yellow denotes $|\downarrow\rangle$). Scale bar, 3 μm. (Image courtesy of C. H. van der Wal, R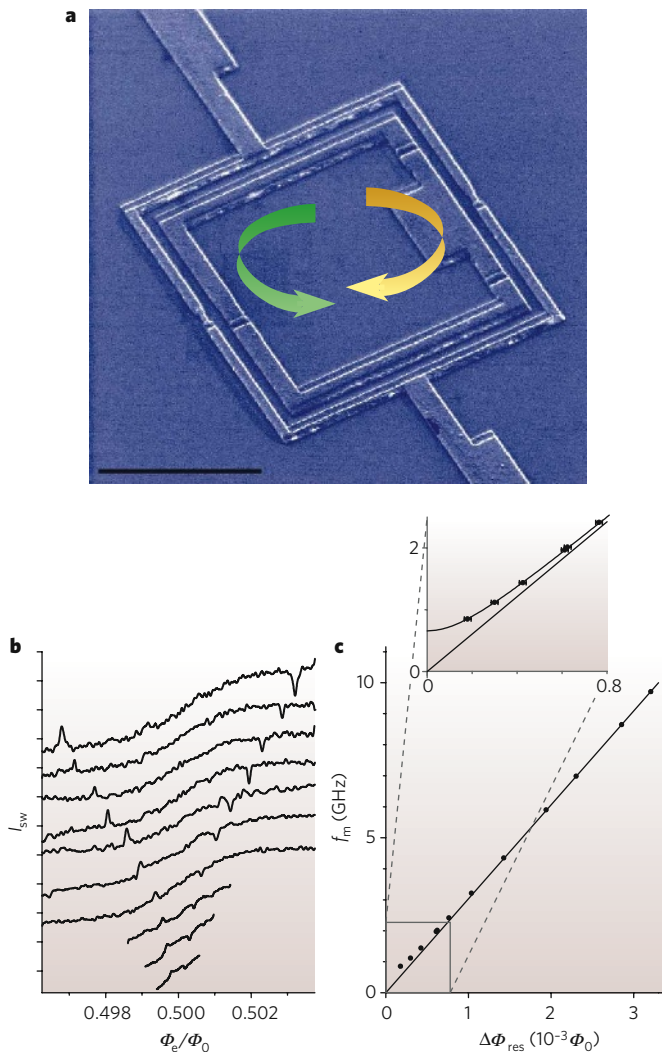ijksuniversiteit Groningen, the Netherlands). **b,** Radiation of microwave frequency f_m induces resonant peaks and dips in the switching current I_{sw} with respect to the externally applied magnetic flux Φ_e normalized to the flux quantum Φ_0. Frequencies range from 9.711 GHz to 0.850 GHz. Tick marks on the y axis show steps of 0.4 nA. (Panel reproduced, with permission, from ref. 15.) **c,** Microwave frequency f_m is plotted against half of the separation in magnetic flux, $\Delta\Phi_{res}$, between the peak and the dip at each frequency. The line is a linear fit through the data at high frequencies and represents the classical energy. The inset is a magnified view of the lower part of the graph; the curved line in the inset is a fit to equation (4). The deviation of the data points from the straight line demonstrates quantum coherence of the $|\uparrow\rangle$ and $|\downarrow\rangle$ flux states. (Panel reproduced, with permission, from ref. 15.)

versus applied flux are shown in Fig. 2b for a succession of microwave frequencies. As expected, the difference in the applied flux at which the peaks and dips appear, $2\Delta\Phi_{res}$, becomes greater as the microwave frequency increases. The microwave frequency versus $\Delta\Phi_{res}$ is shown in Fig. 2c. The data have been fitted to equation (4) with $I_q = (\frac{1}{2})d\nu/d\Phi_e$ in the limit $\nu >> \Delta$, using Δ as a fitting parameter. The data reveal the existence of an anticrossing (that is, an avoided crossing) at $\Phi_e = \Phi_0/2$.

Charge qubits

A charge qubit (also known as a Cooper-pair box) is shown in Fig. 3a, b. The key component is a tiny superconducting island that is small enough that the electrostatic charging energy required to place a charge

of $2e$ on the island at zero voltage, $(2e)^2/2C_\Sigma$, is much greater than the thermal energy k_BT (where $C_\Sigma = C_g + C_j$ is the total capacitance). For $T = 1$ K, this requires C_Σ to be much less than 1 fF. The Cooper-pair box is connected to ground by a gate capacitance C_g in series with a potential V_g and by a small Josephson junction with $E_j << E_c$. Given their weak connection to the 'outside world', the number of Cooper pairs on the island is a discrete variable n. The qubit states correspond to adjacent Cooper-pair number states $|n\rangle$ and $|n+1\rangle$.

To understand how to control a single Cooper pair, it is useful to first examine the electrostatic problem with an infinite junction resistance ($E_j = 0$). The total electrostatic energy of the circuit is $E_{ch} = (2e^2/C_g)(n - n_g)^2$, where $n_g = C_gV_g/2e$ (representing the gate voltage in terms of the gate charge, namely the polarization charge that the voltage induces on the gate capacitor). Although n is an integer, n_g is a continuous variable. E_{ch} versus n_g is shown in Fig. 3c for several values of n. It should be noted that the curves for n and $n+1$ cross at $n_g = n + \frac{1}{2}$, the charge degeneracy point. At this point, the gate polarization corresponds to half a Cooper pair for both charge basis states.

By restoring the Josephson coupling to a small value, the behaviour close to these crossing points is modified. The Josephson junction allows Cooper pairs to tunnel onto the island one by one. The resultant coupling between neighbouring charge states $|n\rangle$ and $|n+1\rangle$ makes the quantum superposition of charge eigenstates analogous to the superposition of flux states in equation (3) (identifying $|\downarrow\rangle = |n\rangle$ and $|\uparrow\rangle = |n+1\rangle$). The next excited charge state is higher in energy by E_c and can safely be neglected. At the charge degeneracy point, where the Josephson coupling produces an avoided crossing, the symmetrical and antisymmetrical superpositions are split by an energy E_j. By contrast, far from this point, $E_c >> E_j$, and the eigenstates are very close to being charge states. Again, the energy level structure is analogous to that of flux qubits, with Δ replaced with E_j and ε with $E_c \times (n_g - n - \frac{1}{2})$. Similarly, the probabilities of measuring the ground state or excited state depend on the gate voltage rather than the applied flux.

To make the qubit fully tunable, the Josephson junction is usually replaced by a d.c. SQUID with low inductance ($\beta_L << 1$). E_j is then adjusted by applying the appropriate magnetic flux, which is kept constant throughout the subsequent measurements.

The read-out of a charge qubit involves detecting the charge on the island to a much greater accuracy than $2e$. This is accomplished by using a single-electron transistor (SET), a sensitive electrometer[16]. The SET (Fig. 3d), also based on a tiny island, is connected to two superconducting leads by two Josephson junctions. When the voltages across both junctions are close to the degeneracy point ($n_g = n + \frac{1}{2}$), charges cross the junctions to produce a net current flow through the SET. Thus, the current near the degeneracy points depends strongly on the gate voltage (Fig. 3c). Capacitively coupling the Cooper-pair-box island to the SET island makes a contribution to the SET gate voltage so that the SET current strongly depends on the Cooper-pair-box state. This scheme converts the measurement of charge into a measurement of charge transport through a SET. In fact, for small Josephson junctions, this charge transport is usually dissipative, because the phase coherence is destroyed by environmental fluctuations. Thus, the read-out actually involves measuring the resistance of the SET, which depends on the state of the Cooper-pair box. The preferred read-out device is a radio-frequency SET[17], in which a SET is embedded in a resonant circuit. Thus, the Q of the resonant circuit is determined by the resistance of the SET and ultimately by the charge on the Cooper-pair box. A pulse of microwaves slightly detuned from the resonant frequency is applied to the radio-frequency SET, and the phase of the reflected signal enables the state of the qubit to be determined.

Many of the initial studies of superconducting qubits involved charge qubits. That crossing is avoided at the degeneracy point was first shown spectroscopically by studying a charge qubit[9], and charge measurements revealed the continuous, quantum-rounded form of the transition between quantum states[18]. The coherent oscillations that occur with time at this avoided energy-level crossing were also first discovered by studying a charge qubit[19].

Cooper-pair boxes are particularly sensitive to low-frequency noise from electrons moving among defects (see the section 'Decoherence') and can show sudden large jumps in n_g. The development of more advanced charge qubits such as the transmon[20] and quantronium[12] has greatly ameliorated this problem. The transmon is a small Cooper-pair box that is made relatively insensitive to charge by shunting the Josephson junction with a large external capacitor to increase E_c and by increasing the gate capacitor to the same size. Consequently, the energy bands of the type shown in Fig. 3c are almost flat, and the eigenstates are a combination of many Cooper-pair-box charge states. For reasons that will be discussed later (see the section 'Decoherence'), the transmon is thus insensitive to low-frequency charge noise at all operating points. At the same time, the large gate capacitor provides strong coupling to external microwaves even at the level of a single photon, greatly increasing the coupling for circuit quantum electrodynamics (QED) (see the section 'Quantum optics on a chip').

The principle by which quantronium operates is shown in Fig. 4a, and an actual circuit is shown in Fig. 4b. The Cooper-pair box involves two Josephson junctions, with a capacitance C_g connected to the island separating them. The two junctions are connected across a third, larger, junction, with a higher critical current, to form a closed superconducting circuit to which a magnetic flux Φ_e is applied. The key to eliminating the effects of low-frequency charge and flux noise is to maintain the qubit at the double degeneracy point at which the two qubit states are (to first order) insensitive to these noise sources. To achieve insensitivity to charge noise, the qubit is operated at $n_g = \frac{1}{2}$, where the energy levels have zero slope and the energy-level splitting is E_j (Fig. 3c). Insensitivity to flux noise is achieved by applying an integer number of half-flux quanta to the loop. The success of this optimum working point has been elegantly shown experimentally[21]. The insensitivity to both flux and charge implies, however, that the two states of the qubit cannot be distinguished at the double degeneracy point. To measure the qubit state, a current pulse that moves the qubit away from the flux degeneracy point is applied to the loop, and this produces a clockwise or anticlockwise current in the loop, depending on the state of the qubit. The direction of the current is determined by the third (read-out) junction: the circulating current either adds to or subtracts from the applied current pulse, so the read-out junction switches out of the zero-voltage state at a slightly lower or slightly higher value of the bias current, respectively. Thus, the state of the qubit can be inferred by measuring the switching currents. With the advent of quantronium, much longer relaxation and decoherence times can be achieved than with a conventional Cooper-pair box.
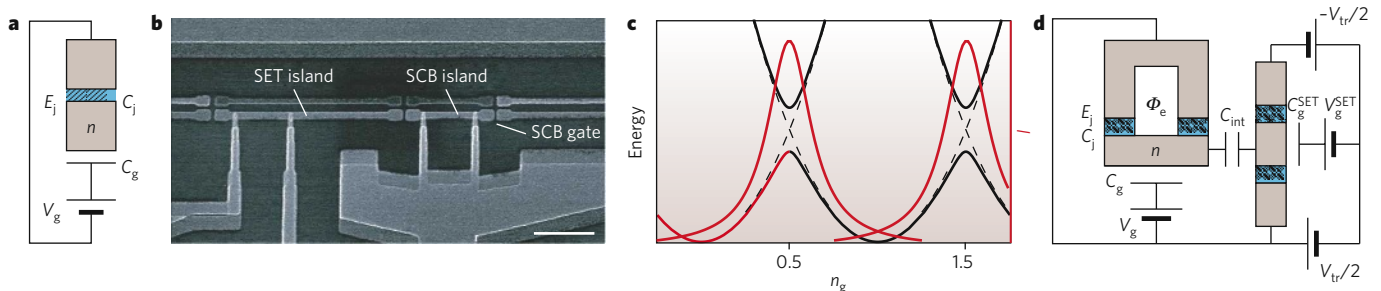
Although this switching read-out scheme is efficient, it has two major drawbacks. First, the resultant high level of dissipation destroys the quantum state of the qubit, making sequential measurements of the state impossible. Second, the temperature of the read-out junction and substrate increase because of the energy that is deposited while the SQUID is in the voltage state — typically for 1 μs — and the equilibrium is not restored for ~1 ms. This limits the rate at which measurements can be made to ~1 kHz, resulting in long data-acquisition times.

These drawbacks have been overcome by the introduction of the Josephson bifurcation amplifier (JBA)[22], a particularly powerful read-out device in which there is no dissipation because the junction remains in the zero-voltage state (Fig. 4c). The JBA exploits the nonlinearity of the Josephson junction when a capacitor is connected across it, resulting in the formation of a resonant (or tank) circuit. When small-amplitude microwave pulses are applied to the resonant circuit, the amplitude and phase of the reflected signal are detected, with the signal strength boosted by a cryogenic amplifier. From this measurement, the resonant frequency of the tank circuit can be determined, then the inductance of the junction — which depends on the current flowing through it — and, finally, the state of the quantronium. For larger-amplitude microwaves, however, the behaviour of the circuit is strongly nonlinear, with the resonance frequency decreasing as the amplitude increases. In particular, strong driving at frequencies slightly below the plasma frequency leads to a bistability: a weak, off-resonance lower branch during which the particle does not explore the nonlinearity, and a high-amplitude response at which frequency matches the driving frequency (Fig. 4d). The two qubit states can be distinguished by choosing driving frequencies and currents that cause the JBA to switch to one response or the other, depending on the qubit state. This technique is extremely fast and, even though it is based on a switching process, it never drives the junction into the voltage state. Furthermore, the JBA remains in the same state after the measurement has been made.

The JBA has been shown to approach the quantum non-demolition (QND) limit[22]. This limit is reached when the perturbation of the quantum state during the measurement does not go beyond that required by the measurement postulate of quantum mechanics, so repeated measurements of the same eigenstate lead to the same outcome[23]. Reaching the QND limit is highly desirable for quantum computing.

A similar scheme that approaches the QND limit has been implemented for the flux qubit, with the single Josephson junction replaced by a read-out SQUID[24]. Dispersive read-out for a flux qubit has also been achieved by inductively coupling a flux qubit to the inductor of a resonant circuit and then measuring the flux state from the shift in the resonance frequency[25].

Figure 3 | Charge qubits. a, A single Cooper-pair-box (SCB) circuit is shown. The superconducting island is depicted in brown and the junction in blue. E_j and C_j are the Josephson coupling energy and self-capacitance, respectively, and n is the number of Cooper pairs on the island, which is coupled to a voltage source with voltage V_g by way of a capacitor with capacitance C_g. (Panel reproduced, with permission, from ref. 28.) **b**, A micrograph of a Cooper-pair box coupled to a single-electron transistor (SET) is shown. Scale bar, 1 μm. (Panel reproduced, with permission, from ref. 78.) **c**, Black curves show the energy of the Cooper-pair box as a function of the scaled gate voltage $n_g = C_g V_g/2e$ for different numbers (n) of excess Cooper pairs on the island. The parabola on the far left corresponds to $n = 0$ and the central parabola to $n = 1$. Dashed lines indicate the contribution of the charging energy $E_{ch}(n, n_g)$ alone. The energy-level splitting at $n_g = \frac{1}{2}$ is E_j. Red curves show the current I through the SET as a function of n_g. Transport is possible at the charge degeneracy points, where the gate strongly modulates the current. (Panel reproduced, with permission, from ref. 28.) **d**, A charge qubit with two junctions (left) coupled to a SET biased to a transport voltage V_{tr} (right) is shown. The critical current of the junctions coupled to the island is adjusted by means of an externally applied magnetic flux Φ_e. The gate of the SET is coupled to an externally controlled charge induced on the capacitor with capacitance C_g^{SET} by the voltage V_g^{SET}, as well as to the qubit charge by way of the interaction capacitance C_{int}. (Panel reproduced, with permission, from ref. 28.)

1035

Phase qubits

In essence, a phase qubit[13] consists of a single current-biased Josephson junction (Box 1 figure). For a bias current I just below the critical current I_0, the anharmonic potential is approximately cubic, and the energy-level spacing becomes progressively smaller as the quantum number n increases. As I approaches I_0, the (classical) plasma oscillation frequency, $\omega_p(I) = 2^{1/4}(2\pi I_0/\Phi_0 C)^{1/2}(1 - I/I_0)^{1/4}$, decreases slowly, while the potential barrier height, $\Delta U(I) = (2\sqrt{2}\, I_0\Phi_0/3\pi)(1 - I/I_0)^{3/2}$, decreases rapidly. Thus, the probability of escape from the state $|n\rangle$ by macroscopic quantum tunnelling increases exponentially as n increases. The qubit involves transitions between the ground state $|0\rangle$ and the first excited state $|1\rangle$. To measure the quantum state of the qubit, a microwave pulse is applied with frequency $(E_2 - E_1)/h$. If, on the one hand, the qubit is in the state $|1\rangle$, then the pulse excites a transition to the state $|2\rangle$, from which macroscopic quantum tunnelling causes the junction to switch to the voltage state. If, on the other hand, the junction is initially in the state $|0\rangle$, then no such transition occurs. Operation of the phase qubit depends crucially on the anharmonicity of the well potential, which ensures that $E_2 - E_1 < E_1 - E_0$.

The first phase qubit that was designed involved a $10 \times 10\,\mu m^2$ Nb–Al$_x$O$_y$–Nb tunnel junction (where $x \leq 2$ and $y \leq 3$), which was created photolithographically. To measure the occupation probability p_1 of the state $|1\rangle$, Martinis et al.[13] applied a long microwave pulse of angular frequency $\omega_{10} = (E_1 - E_0)/\hbar$, followed by a read-out pulse of frequency $\omega_{21} = (E_2 - E_1)/\hbar$ (Fig. 5a). If the state $|1\rangle$ is occupied, the second pulse switches the junction to the voltage state, which is detected by a low-noise amplifier. If, conversely, the junction is in the state $|0\rangle$, the probability of switching is very small. As the power P_{10} in the first pulse is increased, the probability of $|1\rangle$ being occupied increases until it reaches a plateau at 0.5. The results of the measurement are shown in Fig. 5a, where p_1 is defined as the ratio of the number of trials in which switching to the voltage state occurs to the total number of trials. As expected, p_1 approaches 0.5 as P_{10} increases.

In early designs of phase qubits, the junction switched to the voltage state, resulting in energy dissipation. In a later, improved, design[26], the qubits remain in the zero-voltage state (Fig. 5b, c). The qubit junction is embedded in a superconducting loop that is inductively coupled to a SQUID and to a line through which static and pulsed currents can be passed. With appropriately chosen parameters, the potential energy of the qubit displays the two asymmetrical wells shown in Fig. 5c. The states $|0\rangle$ and $|1\rangle$ in the left well are the qubit states; their energy separation and the depth of the well can be controlled by varying the flux in the loop. To read out the state of the phase qubit, a short adiabatic pulse that reduces the depth ΔU of the qubit potential well is applied to the flux bias line. If the qubit is in the state $|1\rangle$, it tunnels rapidly into the right well; in the state $|0\rangle$, no tunnelling occurs. Depending on whether tunnelling occurs, the flux in the qubit loop differs by a single flux quantum, which can easily be detected subsequently by the read-out SQUID. This scheme enables the state of the qubit to be measured rapidly, typically in 5 ns, which is still adiabatic (slow) on the timescale of transitions between the qubit states. Subsequent measurement of the flux in these qubit loops can be made much more slowly.

Time-domain measurements

Spectroscopy is important for establishing that a given qubit is a functional device, and it enables energy-level splitting to be measured as a function of relevant control parameters. But measurements in the
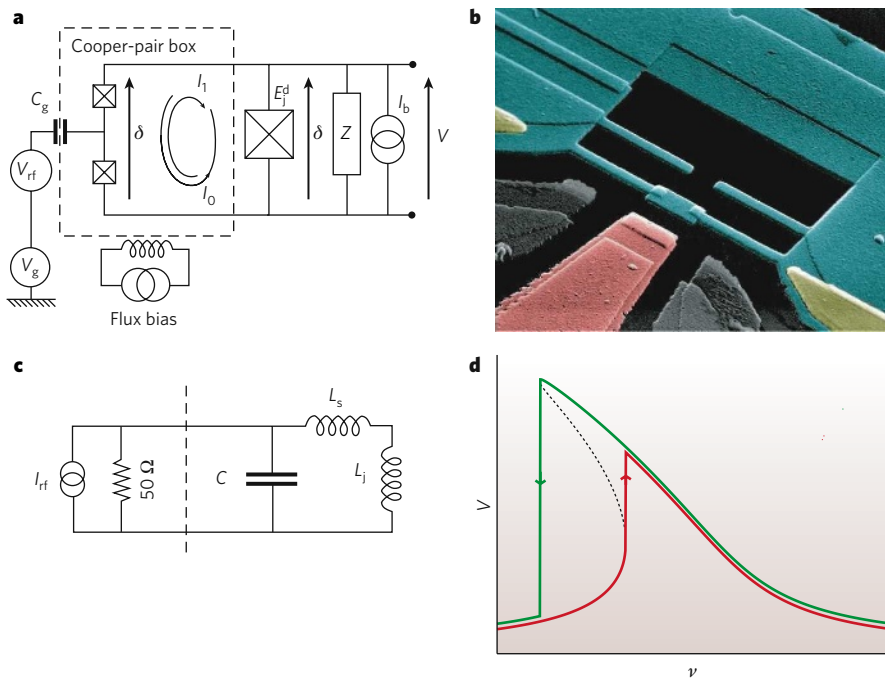

Figure 4 | Quantronium. a, A quantronium circuit is depicted. The Cooper-pair box is connected by way of two Josephson junctions to the detector Josephson junction, which has Josephson energy E^d_j (right), and by way of a capacitor (with gate capacitance C_g) to the static voltage bias V_g and the radio-frequency gate voltage V_{rf} that prepares the state of the Cooper-pair box. The dashed lines enclose the qubit. I_b is the bias current of the detector junction, and Z is an engineered environmental impedance. The flux through the loop formed by the three Josephson junctions is controlled by an external bias circuit. The read-out is the phase δ across the two box junctions, measured by combining the bias current I_b with the circulating loop currents I_0 or I_1. (Panel reproduced, with permission, from ref. 12.) **b**, A micrograph of quantronium is shown. The Cooper-pair box and leads are depicted in blue, and the gate electrode in red. (In gold are normal metal films that are used to remove quasiparticles from the superconducting films.) (Image courtesy of D. Esteve, Commissariat à l'Énergie Atomique, Saclay, France.) **c**, A Josephson bifurcation amplifier (JBA) is depicted. In a JBA, a Josephson junction, represented by the nonlinear inductance L_j, is shunted with a capacitance C via a stray inductance L_S; I_{rf} is the radio-frequency current bias. The dashed line separates the off-chip circuitry (left) from the on-chip circuitry (right). (Panel reproduced, with permission, from ref. 22.) **d**, The response curve (voltage V versus frequency v) of the JBA driven at high radio-frequency current amplitude at a frequency slightly below resonance is shown, and the hysteresis that results from dynamical bifurcation is indicated (arrows). The red line shows the low-amplitude response of the JBA, and the green line shows the high-amplitude response; the dashed line indicates metastable states.

time domain are also necessary to determine the dynamical behaviour of a qubit. These measurements involve manipulating the state of the qubit by using appropriate microwave pulses — which are also required to implement single-qubit gates for quantum computing. In broad terms, qubits are characterized by two times, named T_1 and T_2 by analogy with nuclear magnetic resonance (NMR) spectroscopy[27]. The relaxation time T_1 is the time required for a qubit to relax from the first excited state to the ground state; this process involves energy loss. The dephasing time T_2 is the time over which the phase difference between two eigenstates becomes randomized. Theoretically, both relaxation and dephasing are described by weak coupling to the quantum noise produced by the environment[27–29]. This approach predicts that energy relaxation arises from fluctuations at the energy-level splitting frequency of the two states in question. The dephasing rate, by contrast, has two contributions:

$$1/T_2 = 1/(2T_1) + 1/\tau_\phi \qquad (5)$$

The first contribution arises from the relaxation process, and the second, 'pure dephasing', arises from low-frequency fluctuations with exchange of infinitesimal energy. (The pure dephasing time is τ_ϕ.)

The simplest way to measure relaxation is to irradiate the qubit with microwaves at the frequency corresponding to the energy-level splitting between the ground and first excited states for a time much greater than T_1. After the pulse has been turned off, the qubit has an equal probability of being in either state; the probability p_1 of its being in the excited state $|1\rangle$ subsequently decays with time t as $\exp(-t/T_1)$. Measurements of p_1 as a function of t yield the value of T_1. It should be emphasized that each measurement of p_1 at a given time delay involves a large number of measurements, typically 10^4 or 10^5. T_1 can vary from values of the order of 1 ns to many microseconds.

To understand the various pulse measurements, it is useful to consider the Bloch sphere (Fig. 6a), which enables any arbitrary quantum superposition of the quantum states $|0\rangle$ and $|1\rangle$ to be considered as a vector. The states $|0\rangle$ and $|1\rangle$ point along the positive and negative z axis, respectively. The superpositions $|0\rangle \pm |1\rangle$ lie along the $\pm x$ axes, and the superpositions $|0\rangle \pm i|1\rangle$ along the $\pm y$ axes. Thus, a given point on the surface of the sphere defines a specific superposition of these states.

The Bloch sphere can be used to describe Rabi oscillations in a flux qubit. Microwaves are applied at the energy-level splitting frequency for the qubit for a time τ with the magnetic-field component along the y axis. During the pulse, the state vector rotates in the y–z plane about the x axis with the Rabi frequency ν_R, which is proportional to the microwave

amplitude. After time τ, the state vector is at an angle $2\pi\nu_R\tau$ to the z axis. Subsequent measurements of the probability of the qubit being in the state $|0\rangle$ or $|1\rangle$ yield Rabi oscillations as a function of τ. An example is shown in Fig. 6b. Rabi oscillations are a convenient means of calibrating the amplitude of the magnetic-field component of the microwave field that is coupled to the qubit.

In measuring the dephasing time, it is crucial to distinguish T_2 (equation (5)) — an intrinsic timescale for the decoherence of a single qubit — from T_2^*, the result of an ensemble measurement. The ensemble is formed because experiments on a single qubit need to be carried out repeatedly so that sufficiently precise data are acquired. Even though the different measurements are nominally identical, slow fluctuations on the timescale of a single run result in a change in the operating conditions between runs. This reduces the observed coherence time to T_2^* (which is $< T_2$).

T_2^* and T_2 can be measured separately: T_2^*, which includes the effects of low-frequency noise, by using Ramsey fringes[30]; and T_2, by using a spin-echo technique[27], which eliminates certain low-frequency contributions. To observe Ramsey fringes, a $\pi/2$ microwave pulse is first applied at a frequency f_m — with amplitude calibrated from the Rabi oscillations — that tips the qubit state vector into the equatorial (x–y) plane. The vector precesses freely on the Bloch sphere around the static magnetic field B_0, with a magnitude that decreases with time, owing to dephasing. After a variable time delay τ_d, a second $\pi/2$ microwave pulse brings the state vector to a point on the Bloch sphere that depends on both f_m and τ_d. The subsequent measurement of the qubit state projects the vector onto either $|0\rangle$ or $|1\rangle$. Thus, a plot of the switching probability versus τ_d for a given microwave frequency maps out the free evolution of the qubit. For a resonant pulse ($f_m = \nu_{10}$), the free evolution and the microwave pulses are synchronized, and the measurement reveals a coherence amplitude that decays exponentially with characteristic time T_2^*. To map out T_2^* over a larger parameter space, the $\pi/2$ microwave pulses are detuned from ν_{10}. Thus, the pulse and evolution are no longer synchronized, and oscillations — Ramsey fringes — are observed at a frequency $\nu_{Ramsey} = |f_m - \nu_{10}|$ (Fig. 6c).

To remove the slow fluctuations that differentiate T_2^* from T_2, a spin-echo technique, analogous to that used in NMR, can be used. In this technique, a π pulse is applied at the midpoint in time between the two $\pi/2$ pulses. The π pulse flips the qubit state vector to the opposite side of the equatorial plane; therefore, a fluctuation that initially caused the phase to advance now causes it to lag, and vice versa. Thus, at the time of the second $\pi/2$ pulse, the effects of fluctuations that occur on timescales longer than the overall measurement time are (ideally) completely cancelled out. An example is shown in Fig. 6d.
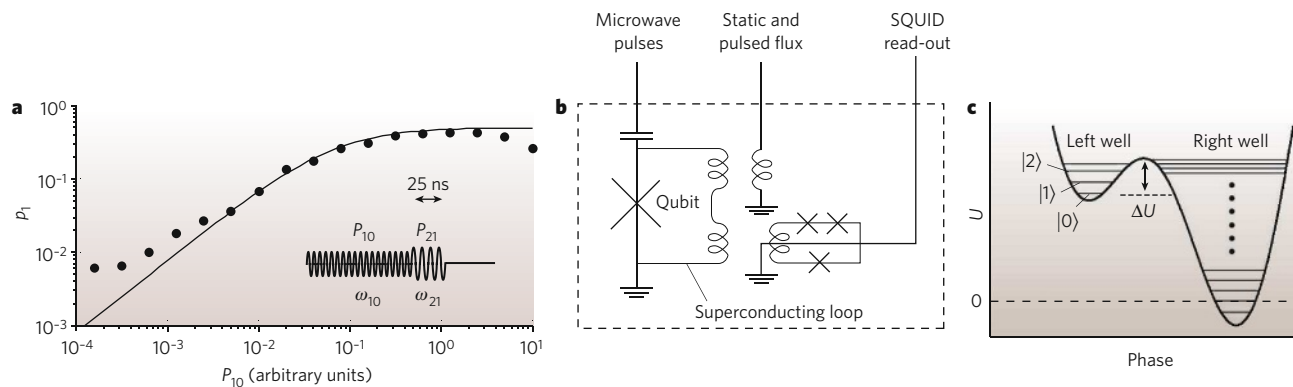

Figure 5 | Phase qubits. a, The filled circles represent the probability p_1 that the phase qubit occupies the first excited state versus microwave power P_{10} at angular frequency ω_{10}. The solid line is the theoretical prediction. The inset shows the pulse sequence; the microwaves at angular frequency ω_{10} equalize the probability that the ground and excited states are occupied, and the microwaves at angular frequency ω_{21} cause the qubit to switch to the voltage state if the first excited state is occupied. (Panel reproduced, with permission, from ref. 13.) **b,** For zero-voltage operation, the Josephson junction of a phase qubit is shunted by a superconducting loop, coupled to a read-out SQUID, that allows static and pulsed fluxes to be applied. The dashed line indicates the components fabricated on the silicon chip, which is maintained at 25 mK. (Panel reproduced, with permission, from ref. 26.) **c,** The asymmetrical double-well potential of a phase qubit is shown. The qubit states are $|0\rangle$ and $|1\rangle$. The state $|2\rangle$ becomes occupied on the application of microwaves at frequency ω_{21} provided that the state $|1\rangle$ is occupied. The state $|3\rangle$, above $|2\rangle$, has no role in the read-out process. Dots in the right well indicate the intervening energy levels. (Panel reproduced, with permission, from ref. 26.)
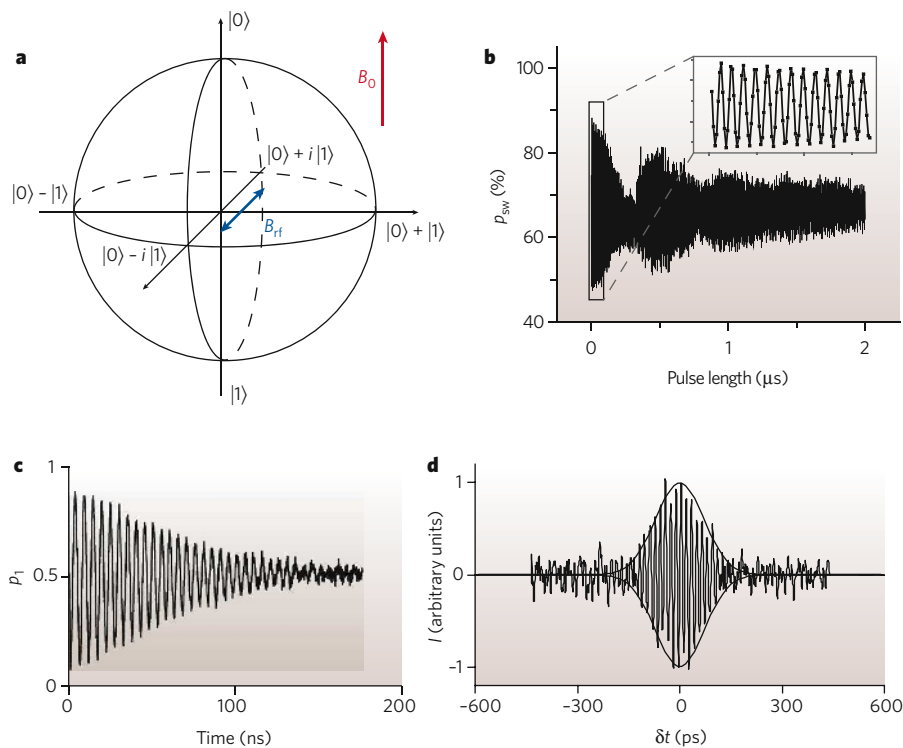
Figure 6 | Qubit manipulation in the time domain. a, The Bloch sphere is depicted, with an applied static magnetic field B_0 and a radio-frequency magnetic field B_{rf}. Any given superposition of the six states shown is represented by a unique point on the surface of the sphere. **b**, Rabi oscillations in a flux qubit are shown. The probability p_{sw} that the detector (SQUID) switches to the normal state versus pulse length is shown, and the inset is a magnification of the boxed region, showing that the dense traces are sinusoidal oscillations. As expected, the excited-state population oscillates under resonant driving. (Panel reproduced, with permission, from ref. 40.) **c**, Ramsey fringes in a phase qubit are shown. Coherent oscillations of the switching probability p_1 between two detuned $\pi/2$ pulses is shown as a function of pulse separation. (Panel reproduced, with permission, from ref. 31.) **d**, The charge echo in a Cooper-pair box is shown as a function of the time difference $\delta t = t_1 - t_2$, where t_1 is the time between the initial $\pi/2$ pulse and the π pulse, and t_2 is the time between the π pulse and the second $\pi/2$ pulse. The echo peaks at $\delta t = 0$. (Panel reproduced, with permission, from ref. 39.)

Measuring the times T_1, T_2 and $T_2^\star$ provides an important initial characterization of qubit coherence. However, other factors such as pulse inaccuracy, relaxation during measurement and more complex decoherence effects result in measurement errors. A more complete measure of a qubit is fidelity, a single number that represents the difference between the ideal and the actual outcome of the experiment. Determining the fidelity involves quantum-process tomography (a repeated set of state tomographies), which characterizes a quantum-mechanical process for all possible initial states. In a Ramsey-fringe tomography experiment, Matthias Steffen et al.[31] found a fidelity of ~80%, where 10% of the loss was attributed to read-out errors and another 10% to pulse-timing uncertainty.

Decoherence

Superconducting qubits are macroscopic, so — along the lines of Schrödinger's cat — they could be expected to be very sensitive to decoherence. In fact, given the unique properties of the superconducting state, careful engineering has led to remarkable increases in decoherence times compared with those of early devices.

Ideally, each type of qubit is described by a single degree of freedom. The central challenge is to eliminate all other degrees of freedom. In broad terms, there are two classes of decohering element: extrinsic and intrinsic. Obvious extrinsic sources include electromagnetic signals from radio and television transmitters; these can generally be eliminated by using careful shielding and enough broadband filters. A more challenging extrinsic source to exclude is the local electromagnetic environment: for example, contributions from the leads that are coupled to read-out devices or are used to apply flux or charge biases. These leads allow great flexibility in control of the system at the expense of considerable coupling to the environment. This issue was recognized in the first proposals of macroscopic quantum coherence and largely motivated the Caldeira–Leggett theory of quantum dissipation[6]. This theory maps any linear dissipation onto a bath of harmonic oscillators. The effects of these oscillators can be calculated from the Johnson–Nyquist noise that is generated by the complex impedance of the environment. In the weak-damping regime, both T_1 and τ_ϕ can be computed directly from the power spectrum of this noise, and then the impedance can be engineered to minimize decoherence[28,29]. The experimental difficulty is to ensure that the complex impedances 'seen' by the qubit are high over a broad bandwidth, for example,

0–10 GHz. It is particularly difficult to avoid resonances over such a broad range of frequencies. Clever engineering has greatly reduced this source of decoherence, but it would be optimistic to consider that this problem has been completely solved.

The main intrinsic limitation on the coherence of superconducting qubits results from low-frequency noise, notably '1/f noise' (in which the spectral density of the noise at low frequency f scales as $1/f^\alpha$, where α is of the order of unity). In the solid state, many 1/f noise sources are well described by the Dutta–Horn model as arising from a uniform distribution of two-state defects[32]. Each defect produces random telegraph noise, and a superposition of such uncorrelated processes leads to a 1/f power spectrum. There are three recognized sources of 1/f noise. The first is critical-current fluctuations, which arise from fluctuations in the transparency of the junction caused by the trapping and untrapping of electrons in the tunnel barrier[33]. All superconducting qubits are subject to dephasing by this mechanism. The slow fluctuations modulate energy-level splitting, even at the degeneracy point, so each measurement is made on a qubit with a slightly different frequency. The resultant phase errors lead to decoherence.

The second source of 1/f noise is charge fluctuations, which arise from the hopping of electrons between traps on the surface of the superconducting film or the surface of the substrate. This motion induces charges onto the surface of nearby superconductors. This decoherence mechanism is particularly problematic for charge qubits, except at the degeneracy point, where the qubits are (to first order) insensitive. If the value of E_c/E_J increases, however, the energy bands (Fig. 3c) become flatter, and the qubit is correspondingly less sensitive to charge noise away from the degeneracy point. This mechanism underlies the substantially increased values of T_2 in the transmon[20].

The third source of 1/f noise is magnetic-flux fluctuations. Although such fluctuations were first characterized more than 20 years ago[34], the mechanism by which these occur remained obscure until recently. It is now thought that flux noise arises from the fluctuations of unpaired electron spins on the surface of the superconductor or substrate[35,36], but the details of the mechanism remain controversial. Flux noise causes decoherence in flux qubits, except at the degeneracy point, as well as in phase qubits, which have no degeneracy point. The increased value of T_2 in quantronium results from its insensitivity to both flux noise and charge noise at the double degeneracy point.

Table 1 | Highest reported values of T_1, $T_2^\star$ and T_2

Qubit	T_1 (μs)	$T_2^\star$ (μs)	T_2 (μs)	Source
Flux	4.6	1.2	9.6	Y. Nakamura, personal communication
Charge	2.0	2.0	2.0	ref. 77
Phase	0.5	0.3	0.5	J. Martinis, personal communication

In general, all three low-frequency processes lead to decoherence. They do not contribute to relaxation because this process requires an exchange of energy with the environment at the energy-level splitting frequency of the qubit, which is typically in the gigahertz range. However, there is strong evidence that charge fluctuations are associated with the high-frequency resonators that have been observed, in particular, in phase qubits[37]. Improvements in the quality of the oxide layers that are used in the junctions and capacitors have resulted in large reductions in the concentration of these high-frequency resonators[38].

The strategy of operating a qubit at the optimum point, which was first carried out with quantronium but is now applied to all types of superconducting qubit (except for phase qubits), has been successful at increasing phase-coherence times by large factors. Further substantial improvements have resulted from the use of charge- or flux-echo techniques[39,40]. In NMR, the spin-echo technique removes the inhomogeneous broadening that is associated with, for example, variations in magnetic field, and hence in the NMR frequency, over the sample. In the case of qubits, the variation is in the qubit energy-level splitting frequency from measurement to measurement. For some qubits, using a combination of echo techniques and optimum point operation has eliminated pure dephasing, so decoherence is limited by energy relaxation ($T_2^\star = 2T_1$). In general, however, the mechanisms that limit T_1 are unknown, although resonators that are associated with defects may be responsible[36,41]. The highest reported values of T_1, $T_2^\star$ and T_2 are listed in Table 1.

Coupled qubits

An exceedingly attractive and unique feature of solid-state qubits in general and superconducting qubits in particular is that schemes can be implemented that both couple them strongly to each other and turn off their interaction *in situ* by purely electronic means. Because the coupling of qubits is central to the architecture of quantum computers, this subject has attracted much attention, in terms of both theory and experiment. In this section, we illustrate the principles of coupled qubits in terms of flux qubits and refer to analogous schemes for other superconducting qubits.

Because the flux qubit is a magnetic dipole, two neighbouring flux qubits are coupled by magnetic dipole–dipole interactions. The coupling
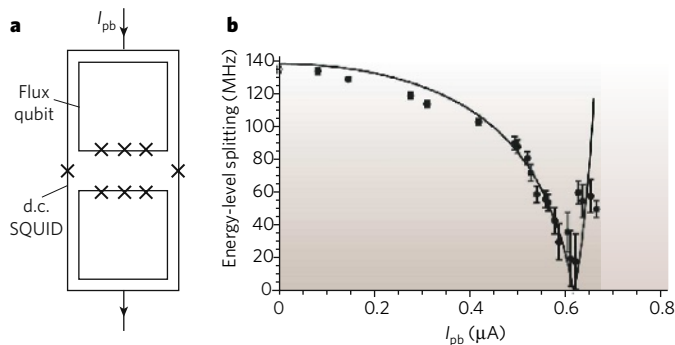
strength can be increased by having the two qubits use a common line. Even stronger coupling can be achieved by including a Josephson junction in this line to increase the line's self-inductance (equation (6), Box 1). In the case of charge and phase qubits, nearest-neighbour interactions are mediated by capacitors rather than inductors. Fixed interaction has been implemented for flux, charge and phase qubits[42–45]. These experiments show the energy levels that are expected for the superposition of two pseudospin states: namely, a ground state and three excited states; the first and second excited states may be degenerate. The entanglement of these states for two phase qubits has been shown explicitly by means of quantum-state tomography[46]. The most general description (including all imperfections) of the qubit state based on the four basis states of the coupled qubits is a four-by-four array known as a density matrix. Steffen *et al.*[46] carried out a measurement of the density matrix; they prepared a system in a particular entangled state and showed that only the correct four matrix elements were non-zero — and that their magnitude was in good agreement with theory. This experiment is a proof-of-principle demonstration of a basic function required for a quantum computer. Simple quantum gates have also been demonstrated[47,48].

Two flux qubits can be coupled by flux transformers — in essence a closed loop of superconductor surrounding the qubits — enabling their interaction to be mediated over longer distances. Because the superconducting loop conserves magnetic flux, a change in the state of one qubit induces a circulating current in the loop and hence a flux in the other qubit. Flux transformers that contain Josephson junctions enable the interaction of qubits to be turned on and off *in situ*. One such device consists of a d.c. SQUID surrounding two flux qubits[49] (Fig. 7a). The inductance between the two qubits has two components: that of the direct coupling between the qubits, and that of the coupling through the SQUID. For certain values of applied bias current (below the critical current) and flux, the self-inductance of the SQUID becomes negative, so the sign of its coupling to the two qubits opposes that of the direct coupling. By choosing parameters appropriately, the inductance of the coupled qubits can be designed to be zero or even have its sign reversed. This scheme has been implemented by establishing the values of SQUID flux and bias current and then using microwave manipulation and measuring the energy-level splitting of the first and second excited states[50] (Fig. 7b). A related design — tunable flux–flux coupling mediated by an off-resonant qubit — has been demonstrated[51], and tunable capacitors have been proposed for charge qubits[52].

Another approach to variable coupling is to fix the coupling strength geometrically and tune it by frequency selection. As an example, we consider two magnetically coupled flux qubits biased at their degeneracy points. If each qubit is in a superposition of eigenstates, then its magnetic flux oscillates and the coupling averages to zero — unless both qubits oscillate at the same frequency, in which case the qubits are coupled. This phenomenon is analogous to the case of two pendulums coupled by a weak spring. Even if the coupling is extremely weak, the pendulums will be coupled if they oscillate in antiphase at exactly the same frequency.

Implementing this scheme is particularly straightforward for two phase qubits because their frequencies can readily be brought in and out of resonance by adjusting the bias currents[37]. For other types of qubit, the frequency at the degeneracy point is set by the as-fabricated parameters, so it is inevitable that there will be variability between qubits. As a result, if the frequency difference is larger than the coupling strength, the qubit–qubit interaction cancels out at the degeneracy point. Several pulse sequences have been proposed to overcome this limitation[53–55], none of which has been convincingly demonstrated as yet. The two-qubit gate demonstrations were all carried out away from the optimum point, where the frequencies can readily be matched.

On the basis of these coupling schemes, several architectures have been proposed for scaling up from two qubits to a quantum computer. The central idea of most proposals is to couple all qubits to a long central coupling element, a 'quantum bus'[56,57] (Fig. 8), and to use frequency selection to determine which qubits can be coupled[56–60]. This scheme has been experimentally demonstrated. As couplers become longer, they become transmission lines that have electromagnetic modes. For example, two

Figure 7 | Controllably coupled flux qubits. a, Two flux qubits are shown surrounded by a d.c. SQUID. The qubit coupling strength is controlled by the pulsed bias current I_{pb} that is applied to the d.c. SQUID before measuring the energy-level splitting between the states $|1\rangle$ and $|2\rangle$. **b,** The filled circles show the measured energy-level splitting of the two coupled flux qubits plotted against I_{pb}. The solid line is the theoretical prediction, fitted for I_{pb}; there are no fitted parameters for the energy-level splitting. Error bars, ±1σ. (Panels reproduced, with permission, from ref. 50.)
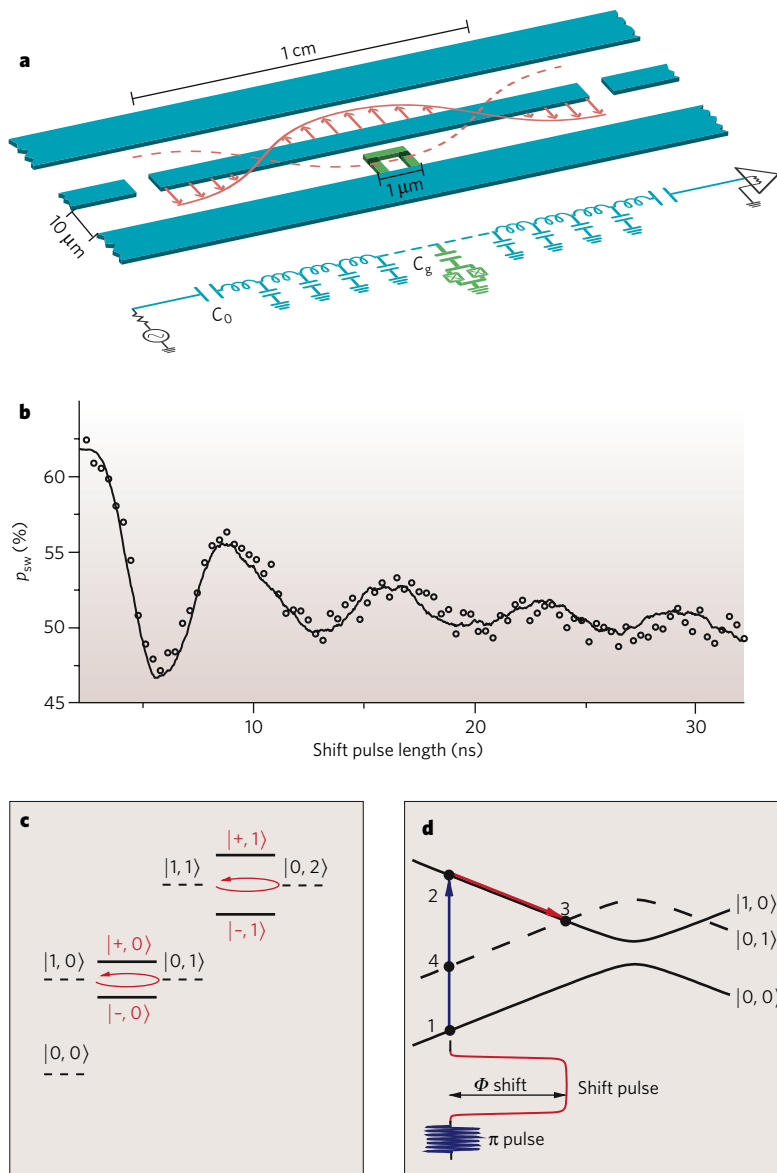
1039

Figure 8 | Circuit QED. a, The upper part of the panel depicts a microstrip cavity (blue) that contains a charge qubit (green) placed at an antinode of the electric field. The microstripline can be used as a quantum bus. The lower part depicts this circuit in a lumped circuit representation. (Panel reproduced, with permission, from ref. 59.) C_0 is the capacitance of the coupling capacitor to the measurement electronics, and C_g is the capacitance of the coupling capacitor to the charge qubit. **b,** The open circles show the measured vacuum Rabi oscillations of a flux qubit coupled to a lumped resonator. The solid curve is a fit to the data. (Panel reproduced, with permission, from ref. 68.) **c,** An energy ladder of qubit ground and excited states combined with photon number n, $|0, n\rangle$ and $|1, n\rangle$ (dashed lines), is shown. With the cavity in resonance with the qubits, the states with zero photons split into linear combinations $|\pm, 0\rangle$ (solid lines), with an energy-level splitting g, and the states with one photon split into linear combinations $|\pm, 1\rangle$, with an energy-level splitting $\sqrt{2}g$. The red arrows indicate that if the system is initially in one of the states represented by dashed lines, it will perform Rabi oscillations between the qubit and the cavity. (Panel modified, with permission, from ref. 68.) **d,** An energy-band diagram (solid and dashed black lines) is shown as a function of applied flux for the measurement scheme that led to the results in **b**. The measurement pulse (π pulse) forces the system from the ground state (point 1) into a state with an excited qubit (point 2) (depicted in blue), which then puts the qubit and the cavity into resonance at point 3 (depicted in red). After the vacuum Rabi oscillation occurs, the system returns to point 2 or makes a coherent transition to point 4, where the qubit excitation is converted to a cavity photon. (Panel modified, with permission, from ref. 68.)

qubits have been coupled by placing them at the antinodes of a standing wave on a stripline[59–62]. Coupling between specific pairs of qubits can result in a scalable architecture[63]. By first coupling a qubit to the standing-wave mode using frequency selection, a photon is excited and then stored after decoupling. Subsequently, a second qubit is coupled to the mode, and the photon transfers the quantum state to the second qubit.

Architectures for adiabatic quantum computers are the subject of intense research. Adiabatic quantum computing encodes the solution to a hard problem in the ground state of a qubit system and uses quantum physics to prepare that ground state efficiently. The ground state of a four-qubit system with tunable interactions has been mapped out[64]. It should, however, be noted that there is no proof that an adiabatic quantum computer will be faster than a classical computer.

Quantum optics on a chip

An important new direction in superconducting qubit research is based on analogy between superconducting circuits and the fields of atomic physics and quantum optics. So far, we have described only qubits as quantum objects, and the control fields and read-out signals have been treated as classical variables. Circuit QED, by contrast, addresses the quantum behaviour of the electromagnetic field, such as that of single photons. In previous sections, the discussion refers to a quantum field in a coherent state in the limit of large numbers of photons.

The key requirement for reaching the quantum limit of the electromagnetic field is that the zero-point fluctuation of a single mode — measured by the root mean square of the electric field, $E_{rms} = \sqrt{\langle E^2 \rangle_{vacuum}}$ — be strong enough to have an appreciable coupling strength $g = dE_{rms}$ to the qubit electric dipole moment d. This requirement is met by increasing the amplitude of the field by creating a standing wave in a resonator and placing the qubit at one of the antinodes[59] (Fig. 8a). The resonator can be either a microstripline — an on-chip wave guide for microwaves — or a lumped circuit. In the first experiment[65], the resonator was tunable. The physics is closely related to cavity QED[66], in which atoms couple to an optical field confined between two mirrors. A key difference is that in circuit QED, the 'atom' (that is, the superconducting qubit) does not move inside the cavity, so the 'atom'–field interaction has time to act without losing the 'atom'. Together with the fact that $g/\hbar$ is larger than the rate of photon loss from the cavity, this difference allows the strong coupling limit of QED to be achieved in a relatively straightforward manner. The underlying reasons are that g is proportional to d (which, for a Cooper-pair box, is large, about 10^4 atomic units) and that E_{rms} is also large because of the increase in the electromagnetic field in the one-dimensional stripline.

Circuit QED can be operated in two distinct strong-coupling limits: the resonant regime, and the off-resonant dispersive regime. In the resonant regime, the qubit energy-level splitting is in resonance with the cavity

frequency. In this regime, the combined states of the qubit and cavity can be written in the form |qubit state, photon number⟩. On resonance, the qubit and cavity can exchange excitations without losing energy: that is, the energy of $|1, n⟩$ is equal to the energy of $|0, n+1⟩$. The eigenstates of the system are thus superpositions of the form $|\pm, n⟩ = |1, n⟩ \pm |0, n+1⟩$, with energies split by $g\sqrt{n}$, leading to the energy spectrum shown in Fig. 8c. This has a striking consequence: suppose that initially the qubit energy is not in resonance with the cavity (so the two are decoupled) and that the qubit is put into an excited state while the cavity is left in its vacuum state. When the qubit and the cavity in that state are suddenly coupled by using the procedure shown in Fig. 8d, the original state ceases to be an eigenstate and, instead, becomes an equal superposition of $|+, 0⟩$ and $|-, 0⟩$. After a time t, these acquire a relative phase of $gt/\hbar$ and manifest themselves as a coherent oscillation between $|1, 0⟩$ and $|0, 1⟩$, even though initially there was no photon in the cavity. These vacuum Rabi oscillations have been shown spectroscopically[67] and in the time domain[68] (Fig. 8b).

The second case is the off-resonant dispersive regime. In this case, the qubit and cavity eigenstates are not entangled, and the two systems cannot share excitations. The mutual energies, however, are still correlated, because the energy-level splitting of the qubit depends on the cavity state, and vice versa. Consequently, the cavity can be used to read out the qubit and to couple qubits to each other[59].

Circuit QED has been highly successful. So far, experimental progress has included attaining the strong coupling limit[67], mapping out the discrete nature of the quantized field[69], generating single photons[70] and coupling qubits using a bus[61,62]. These developments are leading to flexible quantum optics on a chip and open the door to a new domain of mesoscopic physics. Scalable architectures for quantum computers based on circuit QED have been proposed[62].

These ideas have led to the recent demonstration of a superconducting qubit laser. The 'atom' — a charge qubit — is weakly coupled to a second lead. In appropriate bias conditions, a cyclic process takes place: Cooper pairs that enter the box are broken into two quasiparticles, which exit through the second lead. This cycle results in a significant overpopulation of the first excited qubit state compared with the ground state — that is, a population inversion — and the generation of a laser action[71].

Studies in atomic physics have produced superb techniques for actively cooling atoms. Because superconducting qubits operate at millikelvin temperatures, it might be thought that further cooling is unnecessary. But both the preparation of a high-fidelity initial state and the supply of qubits initialized to the ground state for error correction can be facilitated by active cooling. Cooling to 3 mK from an initial temperature of 400 mK has been achieved by exciting the population of the excited state of a flux qubit to a higher excited state that is delocalized in a double-well potential, and then allowing the qubit to relax to the ground state[72]. 'Sisyphus cooling' has also been demonstrated[73]: in this cooling protocol, the energy that is supplied to the qubit from the heat bath is cyclically removed by the magnetic component of a suitably tailored microwave field.

Outlook

Quantum computing is a huge driving force for technological innovation. Since macroscopic quantum coherence was shown, the progress in the design and operation of superconducting qubits has been remarkable. There is now a rich variety of devices that contain the three qubit types, either separately or in combination. Decoherence times have been increased from ~1 ns to ~10 μs, and single-shot and QND read-outs are close to being achieved. So, what challenges and prospects now lie ahead?

On a fundamental level, the next benchmark is to verify a violation of Bell's inequality[74]. This inequality, which involves the outcomes of a combination of two-qubit measurements, is obeyed for any local theory but is violated for truly non-local physics such as quantum mechanics. A variation is the Leggett–Garg inequality[75], which relates to temporal correlations rather than to two-qubit correlations. One important aspect of quantum mechanics — entanglement — has been shown for superconducting qubits[46], but the testing of whether Bell's inequality is violated

poses formidable technological challenges, particularly with respect to the fidelity of the measurement and the elimination of cross-talk. To make a Bell test convincing, the interaction between qubits needs to be switched off very accurately so that measurements are truly independent. An even more convincing test would involve a true space-like separation: that is, measuring the read-out of two qubits in such a short time that no signal has been able to travel between them at the speed of light. Given the confines of a dilution refrigerator, however, it seems that it will not be possible to test superconducting qubits in this way.

Another important experiment involving entanglement will be to investigate whether teleportation of a state occurs[76]: that is, the transfer of a quantum state inside an entangled pair of states.

On the path to quantum computing, superconducting qubits are clearly among the most promising candidates. Nevertheless, the path is long, and there are quantitative technological obstacles to be overcome, notably increasing the decoherence time and improving the fidelity of the read-out. The key benchmark will be to demonstrate simple error correction. To achieve these grand goals will require technological progress, not the least in the elimination — or at least the reduction — of low-frequency noise. Two-qubit coherence — in particular, the question of whether noise processes are correlated between qubits — is largely unexplored.

Will there ever be a superconducting quantum computer? This question cannot be answered today. The error thresholds discussed in fault-tolerance research — 1 error in 10,000 operations being a typical, but by no means universal, benchmark — are daunting. However, fault-tolerance research is an evolving field, and the computational protocols that have been discussed so far (which minimize the number of physical qubits and interactions required for a given algorithm) might not be best suited for superconducting qubits. Promising alternatives might be error-correction models with more generous thresholds, topological computing or other alternative computational models. Adiabatic quantum computing could also be an alternative if it is proved to be faster than classical computing. While addressing these issues, researchers are also likely to gain further insight into many physical properties and processes. ∎

1. Bardeen, J., Cooper, L. N. & Schrieffer, J. R. Theory of superconductivity. *Phys. Rev.* **108,** 1175–1204 (1957).
2. Tinkham, M. *Introduction to Superconductivity* (McGraw-Hill, New York, 1996).
3. Devoret, M. H. in *Quantum Fluctuations: Les Houches Session LXIII* (eds Reynaud, S., Giacobino, E. & David, F.) 351–386 (Elsevier, Amsterdam, 1997).
4. Voss, R. F. & Webb, R. A. Macroscopic quantum tunneling in 1-μm Nb Josephson junctions. *Phys. Rev. Lett.* **47,** 265–268 (1981).
5. Devoret, M. H., Martinis, J. M. & Clarke, J. Measurements of macroscopic quantum tunneling out of the zero-voltage state of a current-biased Josephson junction. *Phys. Rev. Lett.* **55,** 1908–1911 (1985).
6. Caldeira, A. O. & Leggett, A. J. Quantum tunneling in a dissipative system. *Ann. Phys. (NY)* **149,** 374–456 (1983).
7. Martinis, J. M., Devoret, M. H. & Clarke, J. Energy-level quantization in the zero-voltage state of a current-biased Josephson junction. *Phys. Rev. Lett.* **55,** 1543–1546 (1985).
8. Leggett, A. J. in *Chance and Matter: Les Houches Session XLVI* (eds Souletie, J., Vannimenus, J. & Stora, R.) 395–506 (Elsevier, Amsterdam, 1987).
9. Nakamura, Y., Chen, C. D. & Tsai, J. S. Spectroscopy of energy-level splitting between two macroscopic quantum states of charge coherently superposed by Josephson coupling. *Phys. Rev. Lett.* **79,** 2328–2331 (1997).
10. Friedman, J. R., Patel, V., Chen, W., Tolpygo, S. K. & Lukens, J. E. Quantum superpositions of distinct macroscopic states. *Nature* **406,** 43–46 (2000).
11. van der Wal, C. H. *et al.* Quantum superpositions of macroscopic persistent current. *Science* **290,** 773–776 (2000).
12. Vion, D. *et al.* Manipulating the quantum state of an electrical circuit. *Science* **296,** 886–889 (2002).
13. Martinis, J. M., Nam, S., Aumentado, J. & Urbina, C. Rabi oscillations in a large Josephson-junction qubit. *Phys. Rev. Lett.* **89,** 117901 (2002).
14. *The SQUID Handbook: Fundamentals and Technology of SQUIDs and SQUID Systems* Vol. I (eds Clarke, J. & Braginski, A. I.) (Wiley, Weinheim, 2004).
15. Wilhelm, F. K. *et al.* Macroscopic quantum superposition of current states in a Josephson junction loop. *Usp. Fiz. Nauk* **44** (suppl. 171), 117–121 (2001).
16. Devoret, M. H. & Schoelkopf, R. Amplifying quantum signals with the single-electron transistor. *Nature* **406,** 1039–1046 (2000).
17. Schoelkopf, R. J., Wahlgren, P., Kozhevnikov, A. A., Delsing, P. & Prober, D. E. The radio-frequency single-electron transistor (RF-SET): a fast and ultrasensitive electrometer. *Science* **280,** 1238–1242 (1998).
18. Bouchiat, V., Vion, D., Joyez, P., Esteve, D. & Devoret, M. H. Quantum coherence with a single Cooper pair. *Physica Scripta* **T76,** 165–170 (1998).
19. Nakamura, Y., Pashkin, Y. A. & Tsai, J. S., Coherent control of macroscopic quantum states in a single-Cooper-pair box. *Nature* **398,** 786–788 (1999).

20. Koch, J. *et al.* Charge-insensitive qubit design derived from the Cooper pair box. *Phys. Rev. A* **76,** 042319 (2007).
21. Ithier, G. *et al.* Decoherence in a superconducting quantum bit circuit *Phys. Rev. B* **72,** 134519 (2005).
22. Siddiqi, I. *et al.* Direct observation of dynamical bifurcation between two driven oscillation states of a Josephson junction. *Phys. Rev. Lett.* **94,** 027005 (2005).
23. Braginsky, V. B., Khalili, F. Y. & Thorne, K. S. *Quantum Measurement* (Cambridge Univ. Press, Cambridge, UK, 1995).
24. Lupaşcu, A. *et al.* Quantum non-demolition measurement of a superconducting two-level system. *Nature Phys.* **3,** 119–125 (2007).
25. Grajcar, M. *et al.* Low-frequency measurement of the tunneling amplitude in a flux qubit. *Phys. Rev. B* **69,** 060501 (2004).
26. Cooper, K. B. *et al.* Observation of quantum oscillations between a Josephson phase qubit and a microscopic resonator using fast readout. *Phys. Rev. Lett.* **93,** 180401 (2004).
27. Slichter C. P. *Principles of Nuclear Magnetic Resonance* 3rd edn (Springer, New York, 1990).
28. Makhlin, Y., Schön, G. & Shnirman, A. Quantum-state engineering with Josephson-junction devices. *Rev. Mod. Phys.* **73,** 357–400 (2001).
29. Wilhelm, F. K., Hartmann, U., Storcz, M. J. & Geller, M. R. in *Manipulating Quantum Coherence in Solid State Systems* (eds Flatté, M. E. & Tifrea, I.) 195–233 (Springer, Dordrecht, 2007).
30. Ramsey, N. F. A molecular beam resonance method with separated oscillating fields. *Phys. Rev.* **78,** 695–699 (1950).
31. Steffen, M. *et al.* State tomography of capacitively shunted phase qubits with high fidelity. *Phys. Rev. Lett.* **97,** 050502 (2006).
32. Dutta P. & Horn P. M. Low frequency fluctuations in solids: $1/f$ noise. *Rev. Mod. Phys.* **53,** 497–516 (1981).
33. van Harlingen, D. J. *et al.* Decoherence in Josephson-junction qubits due to critical-current fluctuations. *Phys. Rev. B* **70,** 064517 (2004).
34. Wellstood, F. C., Urbina, C. & Clarke, J. Low-frequency noise in dc superconducting quantum interference devices below 1 K. *Appl. Phys. Lett.* **50,** 772–774 (1987).
35. Koch, R. H., DiVincenzo, D. P. & Clarke, J. Model for $1/f$ flux noise in SQUIDs and qubits. *Phys. Rev. Lett.* **98,** 267003 (2007).
36. Faoro, L. & Ioffe, L. B. Microscopic origin of low-frequency flux noise in Josephson circuits. Preprint at <http://arxiv.org/abs/0712.2834> (2007).
37. Simmonds, R. W., Lang, K. M., Hite, D. A., Pappas, D. P. & Martinis, J. M. Decoherence in Josephson qubits from junction resonances. *Phys. Rev. Lett.* **93,** 077033 (2004).
38. Martinis, J. M. *et al.* Decoherence in Josephson qubits from dielectric loss. *Phys. Rev. Lett.* **95,** 210503 (2005).
39. Nakamura, Y., Pashkin, Y. A., Yamamoto, T. & Tsai, J. S. Charge echo in a Cooper-pair box. *Phys. Rev. Lett.* **88,** 047901 (2002).
40. Bertet, P. *et al.* Relaxation and dephasing in a flux-qubit. *Phys. Rev. Lett.* **95,** 257002 (2005).
41. Astafiev, O., Pashkin, Y. A., Nakamura, Y., Yamamoto, T. & Tsai, J. S. Quantum noise in the Josephson charge qubit. *Phys. Rev. Lett.* **93,** 267007 (2004).
42. Berkley, A.J. *et al.* Entangled macroscopic quantum states in two superconducting qubits. *Science* **300,** 1548–1550 (2003).
43. Majer, J. B., Paauw, F. G., ter Haar, A. C. J., Harmans, C. J. P. M. & Mooij, J. E. Spectroscopy of coupled flux qubits. *Phys. Rev. Lett.* **94,** 090501 (2005).
44. Pashkin, Y. A. *et al.* Quantum oscillations in two coupled charge qubits. *Nature* **421,** 823–826 (2003).
45. McDermott, R. *et al.* Simultaneous state measurement of coupled Josephson phase qubits. *Science* **307,** 1299–1302 (2005).
46. Steffen, M. *et al.* Measurement of the entanglement of two superconducting qubits via state tomography. *Science* **313,** 1423–1425 (2006).
47. Yamamoto, Y., Pashkin, Y. A., Astafiev, O., Nakamura, Y. & Tsai, J. S. Demonstration of conditional gate operation using superconducting charge qubits. *Nature* **425,** 941–944 (2003).
48. Plantenberg, J. H., de Groot, P. C., Harmans, C. J. & Mooij, J. E. Demonstration of controlled-NOT quantum gates on a pair of superconducting quantum bits. *Nature* **447,** 836–839 (2007).
49. Plourde, B. L. T. *et al.* Entangling flux qubits with a bipolar dynamic inductance. *Phys. Rev. B* **70,** 140501 (2004).
50. Hime, T. *et al.* Solid-state qubits with current-controlled coupling. *Science* **314,** 1427–1429 (2006).
51. Niskanen, A. O. *et al.* Quantum coherent tunable coupling of superconducting qubits. *Science* **316,** 723–726 (2007).
52. Averin, D. V. & Bruder, C. Variable electrostatic transformer controllable coupling of two charge qubits. *Phys. Rev. Lett.* **91,** 057003 (2003).
53. Bertet, P., Harmans, C. J. P.M. & Mooij, J. E. Parametic coupling for superconducting qubits. *Phys. Rev. B* **73,** 064512 (2006).
54. Rigetti, C., Blais, A. & Devoret, M. Protocol for universal gates in optimally biased superconducting qubits. *Phys. Rev. Lett.* **94,** 240502 (2005).
55. Liu, Y.-x., Wei, L. F., Tsai, J. S. & Nori, F. Controllable coupling between flux qubits. *Phys. Rev. Lett.* **96,** 067003 (2006).
56. Makhlin, Y., Schön, G. & Shnirman, A. Josephson-junction qubits with controlled couplings. *Nature* **398,** 305–307 (1999).
57. Wei, L. F., Liu, Y.-x. & Nori, F. Quantum computation with Josephson qubits using a current-biased information bus. *Phys. Rev. B* **71,** 134506 (2005).
58. Lantz, J., Wallquist, M., Shumeiko, V. S. & Wendin, G. Josephson junction qubit network with current-controlled interaction. *Phys. Rev. B* **70,** 140507 (2004).
59. Blais, A., Huang, R.-S., Wallraff, A., Girvin, S. M. & Schoelkopf, R. J. Cavity quantum electrodynamics for superconducting electrical circuits: an architecture for quantum computation. *Phys. Rev. A* **69,** 062320 (2004).
60. Helmer, F. *et al.* Two-dimensional cavity grid for scalable quantum computation with superconducting circuits. Preprint at <http://arxiv.org/abs/0706.3625> (2007).
61. Majer, J. B. *et al.* Coupling superconducting qubits via a cavity bus. *Nature* **449,** 443–447 (2007).
62. Sillanpaa, M. A., Park, J. I. & Simmonds, R. W. Coherent quantum state storage and transfer between two phase qubits via a resonant cavity. *Nature* **449,** 438–442 (2007).
63. Fowler, A. G. *et al.* Long-range coupling and scalable architecture for superconducting flux qubits. *Phys. Rev. B* **76,** 174507 (2007).
64. Grajcar, M. *et al.* Four-qubit device with mixed couplings. *Phys. Rev. Lett.* **96,** 047006 (2006).
65. Devoret, M. H. *et al.* in *Quantum Tunneling in Condensed Media* (eds Kagan, Y. & Leggett, A. J.) 313–345 (Elsevier, Amsterdam, 1992).
66. Haroche, S. & Kleppner, D. Cavity quantum electrodynamics. *Phys. Today* **42,** 24–26 (1989).
67. Wallraff, A. *et al.* Strong coupling of a single photon to a superconducting qubit using circuit quantum electrodynamics. *Nature* **431,** 162–167 (2004).
68. Johansson, J. *et al.* Vacuum Rabi oscillations in a macroscopic superconducting qubit *LC* oscillator system. *Phys. Rev. Lett.* **96,** 127006 (2006).
69. Schuster, D. I. *et al.* Resolving photon number states in a superconducting circuit. *Nature* **445,** 515–518 (2007).
70. Houck, A. A. *et al.* Generating single microwave photons in a circuit. *Nature* **449,** 443–447 (2007).
71. Astafiev, O. *et al.* Single artificial-atom lasing. *Nature* **449,** 588–590 (2007).
72. Valenzuela, S. O. *et al.* Microwave-induced cooling of a superconducting qubit. *Science* **314,** 1589–1592 (2006).
73. Gracjar, M. *et al.* Sisyphus damping and amplification by a superconducting qubit. Preprint at <http://arxiv.org/abs/0708.0665> (2007).
74. Clauser, J. F., Horne, M. A., Shimony, A. & Holt, R. A. Proposed experiment to test local hidden-variable theories. *Phys. Rev. Lett.* **23,** 880–884 (1969).
75. Leggett, A. J. & Garg, A. Quantum mechanics versus macroscopic realism: is the flux there when nobody looks? *Phys. Rev. Lett.* **54,** 857–860 (1985).
76. Bennett, C. H. *et al.* Teleporting an unknown quantum state via dual classical and Einstein–Podolsky–Rosen channels. *Phys. Rev. Lett.* **70** 1895–1899 (1993).
77. Schreier, J. A. *et al.* Suppressing charge noise decoherence in superconducting charge qubits. *Phys. Rev. B* **77,** 180502 (2008).
78. Duty, T., Gunnarson, D., Bladh, K. & Delsing, P. Coherent dynamics of a Josephson charge qubit. *Phys. Rev. B* **69,** 140503 (2004).
79. Dolan, G. J. Offset masks for liftoff photoprocessing. *Appl. Phys. Lett.* **31,** 337–339 (1977).

Author Information Reprints and permissions information is available at npg.nature.com/reprints. The authors declare no competing financial interests. Correspondence should be addressed to the authors (jclarke@berkeley.edu; fwilhelm@iqc.ca).